Journal of Power Sources 196 (2011) 7245–7250

Contents lists available at ScienceDirect

Journal of Power Sources

journal homepage: www.elsevier.com/locate/jpowsour

$La_2NiO_{4+\delta}$ potential cathode material on $La_{0.9}Sr_{0.1}Ga_{0.8}Mg_{0.2}O_{2.85}$ electrolyte for intermediate temperature solid oxide fuel cell

María José Escudero[a,*], Araceli Fuerte[a], Loreto Daza[a,b]

[a] CIEMAT, Departmento de Energía, Av Complutense 22, 28040 Madrid, Spain
[b] Instituto de Catálisis y Petroleoquímica (CSIC), Marie Curie 2, Campus Cantoblanco, 28049 Madrid, Spain

ARTICLE INFO

Article history:
Received 23 June 2010
Received in revised form 21 October 2010
Accepted 15 November 2010
Available online 20 November 2010

Keywords:
K_2NiF_4
Cathode
Fuel cell
IT-SOFC
LSGM
Electrochemical performance

ABSTRACT

$La_2NiO_{4+\delta}$, a mixed ionic-electronic conducting oxide with K_2NiF_4 type structure, has been studied as cathode material with $La_{0.9}Sr_{0.1}Ga_{0.8}Mg_{0.2}O_{2.85}$ (LSGM) electrolyte for intermediate solid oxide fuel cells (IT-SOFCs). XRD results reveal excellent chemical compatibility between the $La_2NiO_{4+\delta}$ sample and LSGM electrolyte.

A single cell (0.22 cm^2 active area) was fabricated with $La_2NiO_{4+\delta}$ as cathode, Ni–$Sm_{0.2}Ce_{0.8}O_{1.9}$ (2:1; w/w) as anode and LSGM as electrolyte. A thin buffer layer of $Sm_{0.2}Ce_{0.8}O_{1.9}$ (SDC) between anode and electrolyte was used to avoid possible interfacial reactions. The cell was tested under humidified H_2 and stationary air as fuel and oxidant, respectively. The electrochemical behaviour was evaluated by means of current–voltage curves and impedance spectroscopy. Microstructure and morphology of the cell components were analysed by SEM-EDX after testing.

The maximum power densities were 160, 226, and 322 mW cm^{-2} at 750, 800 and 850 °C, respectively with total polarisation resistances of 0.77, 0.48 and 0.31 Ω cm^2 at these temperatures. Cell performance remained stable when a current density of 448 mA cm^{-2} was demanded for 144 h at 800 °C, causing no apparent degradation in the cell. The performance of this material may be further improved by reducing the electrolyte thickness and optimisation of the electrode microstructure.

1. Introduction

Solid oxide fuel cell (SOFC) is one of the most promising highly efficient energy-conversion systems. Currently, one of the critical targets for the commercialization of SOFC devices is to reduce the operation temperature, from above 900 °C to an intermediate temperature range (600–800 °C). However, there are two notable technical challenges in intermediate temperature solid oxide fuel cell (IT-SOFC) development; one is the lower ionic conductivity of the electrolyte and the other is the lower electrochemical activity of electrodes at reduced temperatures [1].

The increase of ohmic loss due to the lower ionic conductivity of the electrolyte may be minimised by using high ionic-conducting materials such as doped ceria, doped lanthanum gallate or scandia-stabilised zirconia. Among these electrolyte materials, Sr and Mg co-doped lanthanum gallate-based electrolytes (LSGM) are most interesting for IT-SOFC, because LSGM exhibits a conductivity several times higher than 8 mol% yttria-stabilised zirconia (YSZ) at temperatures of 650–800 °C [2], comparable to that of gadolinium doped CeO_2, and an ionic transport number close to unity within large ranges of oxygen partial pressure and temperature [3,4]. However, LSGM is known to have higher chemical reactivity with Ni-based cermet anodes [5,6]. The reactivity between LSGM and Ni results in the formation of high-resistivity compounds at the interface such as $LaNiO_3$ and $LaSrGa_3O_7$. These reaction products would lead to the degradation of cell performance because of an anomalous increase in ohmic loss. Some inert buffer layers of $Ce_{0.6}La_{0.4}O_2$ (LDC), $Ce_{0.9}Gd_{0.1}O_{2-\delta}$ (GDC) or $Ce_{0.8}Sm_{0.2}O_{2-\delta}$ (SDC) have been proposed to avoid the formation of undesirable compounds [5–9]. Thus, Yan et al. [9] reported that the incorporation of an interlayer of SDC (400 nm thick) between the anode of NiO–Fe_2O_3–SDC and the LSGM electrolyte avoids the reaction between LSGM and NiO and also promotes the electrode processes.

The polarisation loss of a cell also greatly increases at low temperature, mainly due to the large cathode overpotential. In order to solve this problem, mixed ionic and electronic conducting (MIEC) materials have attracted much attention as potential cathodes for IT-SOFC. It is believed that the improved electrode properties are due to the extended reaction sites from the three phase boundary region (TPB) to the whole electrode surface, consequently the cathode polarisation obviously decreases and enhances the cell performance at reduced temperatures when a MIEC is used as cath-

* Corresponding author. Tel.: +34 913466622, fax: +34 913466269.
E-mail address: m.escudero@ciemat.es (M.J. Escudero).

0378-7753/$ – see front matter © 2010 Elsevier B.V. All rights reserved.
doi:10.1016/j.jpowsour.2010.11.068

ode [10,11]. Most studies concerning MIEC cathode materials deal with perovskite-type oxides [12–18]. In the last decade, a new family of compounds formulated $A_2MO_{4+\delta}$ with the K_2NiF_4-type structure has received much attention as potential cathode materials for IT-SOFC [19–25]. Among the most studied are the pure and doped $La_2NiO_{4+\delta}$ because of their ability to accommodate a large oxygen overstoichiometry. These compounds exhibit a relativity high oxygen-ion diffusivity, thermal expansion coefficients (TECs) compatible with solid electrolytes, predominant *p*-type electronic conductivity in the whole $p(O_2)$ range where the K_2NiF_4-type phases exist, and high electrocatalytic activity [26,27]. Previous studies performed by our group revealed that the $La_2NiO_{4+\delta}$ compound presents an oxygen excess (δ) of 0.17 [28] and exhibits relatively high electrical conductivity, thermal expansion coefficient compatible with yttrium-stabilised zirconia (YSZ) and Sr and Mg co-doped lanthanum gallate (LSGM) electrolytes as well as good electrocatalytic activity for the oxygen reduction on LSGM at intermediate temperatures [29,30].

In this study, the $La_2NiO_{4+\delta}$ compound has been investigated as a cathode material for application in IT-SOFC based on a LSGM electrolyte. The chemical compatibility between $La_2NiO_{4+\delta}$ and LSGM was analysed by X-ray diffraction (XRD). Electrochemical measurements have been performed in single cell to evaluate performance and stability. Post test analyses of cell components have been carried out with a scanning electron microscope and energy-dispersive X-ray spectroscopy (SEM–EDX) in order to study the microstructure and morphology.

2. Experimental

$La_2NiO_{4+\delta}$ powder was synthesised via a nitrate–citrate route as cathode material. Stoichiometric amounts of analytical grade La_2O_3 (98.5%) and $Ni(NO_3)_2{\cdot}6H_2O$ (99%) (Panreac) were dissolved in nitric acid (65%) (Merck). Citric acid (99.5%) (Panreac) was added in a large excess (3.3 moles per mole of nickel nitrate) under continuous stirring. The solution was dehydrated and slowly heated until self-combustion of the precipitate. Precursors obtained by the means were calcined at 600 °C for 2 h and finally fired in air at 950 °C for 8 h [29]. The sample was characterised by X-ray diffraction (XRD) for phase identification and phase purity assesment. XRD analysis was performed with a Philips "X Pert-MPD" diffractometer using Cu K_α radiation (λ = 1.5406 Å). The diffraction patterns were recorded in the 20°–80° 2θ range with a scan step of 0.04°. Chemical compatibility of the $La_2NiO_{4+\delta}$ oxide with the $La_{0.9}Sr_{0.1}Ga_{0.8}Mg_{0.2}O_{3-\delta}$ (LSGM) electrolyte (Praxair) was investigated by mixing the cathode material and electrolyte powders in a 1:1 weight ratio, following by calcination at 1000 °C for 50 h. The resulting mixture was analysed by XRD.

The electrolyte pellet was prepared by uniaxial pressure and calcination at 1500 °C for 10 h from the powder electrolyte. The surface of the electrolyte was roughened by mechanical grinding to reduce its thickness. After sintering, a dense LSGM pellet was obtained with a diameter of ~11 mm and a thickness of ~0.4 mm.

Nickel oxide (NiO, Panreac) and $Sm_{0.2}Ce_{0.8}O_{1.9}$ (SDC, Praxair) were used to prepare the NiO–SDC composite as an anode material. The anode ink was prepared by mixing the powders of NiO and SDC (66.7:33.3 wt.%) in an agate mortar milled with acetone and left to dry in air. After that, a binder (Decoflux, WB41, Zschimmer and Schwartz) was added to obtain a slurry. To prevent the reaction between Ni-SDC and LSGM, a SDC buffer layer was first prepared by painting onto the anode side of the LSGM electrolyte. After heating the buffer layer at 1100 °C for 4 h, the anode ink was painted onto the SDC layer and heated at 1100 °C for 4 h.

The cathode ink was prepared following the same procedure with the $La_2NiO_{4+\delta}$ compound as the material. The cathode ink was deposited on the other side of the electrolyte by painting. After that, the cell was fired at 1000 °C for 4 h with a ramp rate of 2 °C min^{-1}. Finally, Au current collector and Pt current collector was placed on the anode and cathode using Au and Pt inks, respectively, and fired at 900 °C for 2 h. During initial heating, humidified hydrogen (3% H_2O) was supplied in order to reduce the anode NiO–SDC to Ni–SDC cermet.

Cell performance was evaluated using an in-house built test station. The single cell, with an active area of 0.22 cm^2, was sealed into an alumina tube with a ceramic cement (Aremco, Ceramabond 525). Humidified hydrogen (3% H_2O) with a flow rate of 50 ml min^{-1} was fed to the anode chamber, while the cathode was simply exposed to air. Electrochemical measurements were conducted using AUTOLAB system (PGSTAT30 and FRA2 module) from Eco Chemie. The current–voltage (*I–V*) characteristic of the cell was measured using linear sweep voltammetry at a scan rate of 10 mV s^{-1}. The impedance of the cell was recorded at open circuit in galvanostatic mode in a frequency range from 0.1 Hz to 1 MHz and excitation signal of 5 mA.

Microstructure and morphology of the cell and its components were analysed by a scanning electron microscopy (SEM, Hitachi S-2500), equipped with an X-ray analyzer for energy dispersive X-ray (EDX) spectroscopy.

3. Results

XRD patterns of the $La_2NiO_{4+\delta}$ –LSGM mixture calcined at 1000 °C for 50 h are shown in Fig. 1. For comparison, the pattern of the $La_2NiO_{4+\delta}$ and LSGM powders are displayed in the same figure. $La_2NiO_{4+\delta}$ oxide presents a single phase K_2NiF_4-type structure, and no impurities were observed (Fig. 1b). In a previous article [31], we determined its structure from neutron powder diffraction data in the orthorhombic *Fmmm* space group, with unit cell parameters a = 5.4629 Å, b = 5.4612 Å, c = 12.7039 Å and V = 379.01 Å^3 [28]. LSGM powders exhibit single phase perovskite

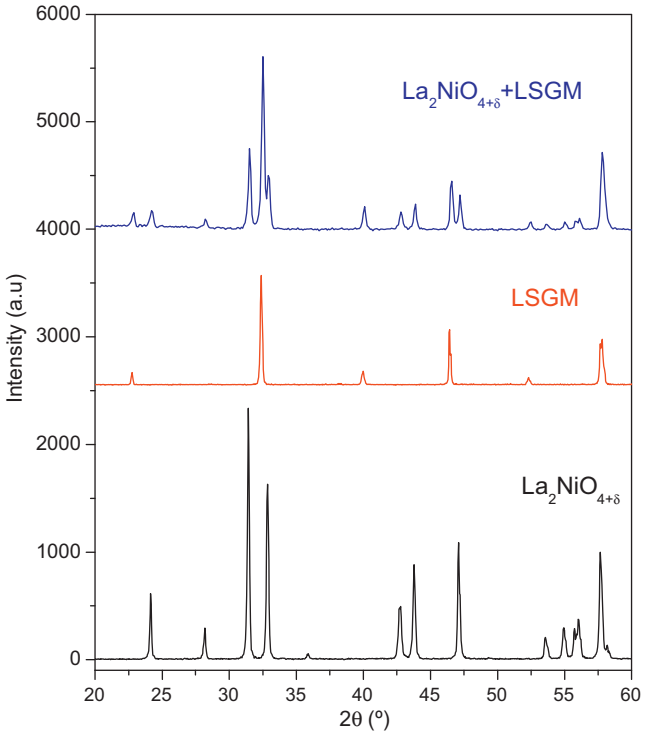

Fig. 1. XRD patterns of $La_2NiO_{4+\delta}$ powders, LSGM powders and the $La_2NiO_{4+\delta}$ –LSGM mixture calcined at 1000 °C for 50 h.

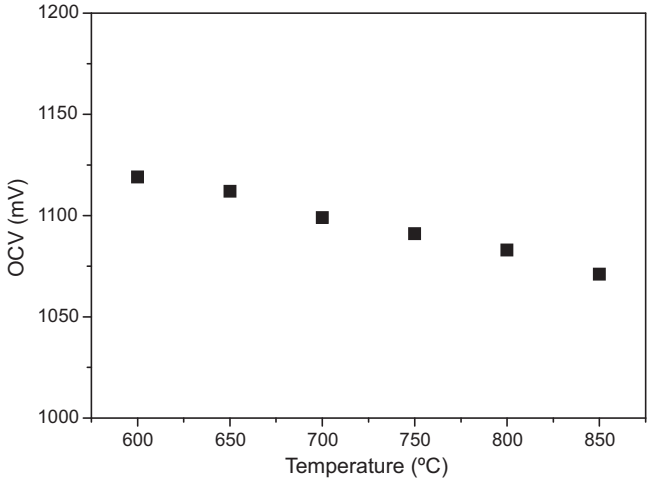

Fig. 2. OCV for the $La_2NiO_{4+\delta}$/LSGM/SDC/Ni–SDC cell in H_2 (3% H_2O) and static air, as function of temperature.

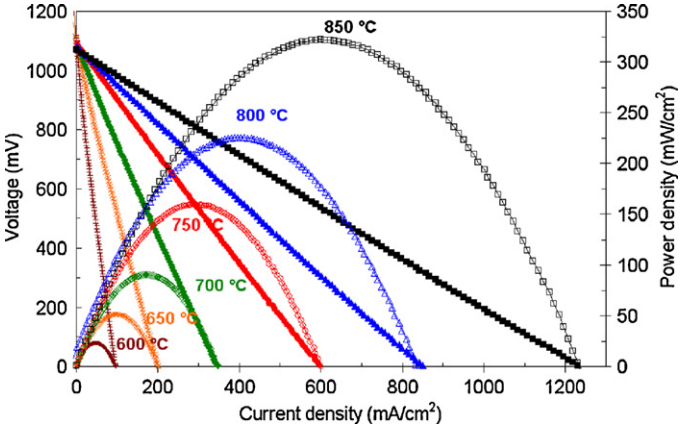

Fig. 3. Voltage and power density versus current density for the $La_2NiO_{4+\delta}$/LSGM/SDC/Ni–SDC cell in H_2 (3% H_2O) and static air at different temperatures.

structure with a cubic symmetry [4,32], and no impurity phases are found in the present sample (Fig. 1a). After the heat treatment of the $La_2NiO_{4+\delta}$ –LSGM mixture both compounds still retain their structures. Clearly, no new identifiable peaks or shift of XRD peaks were observed in the pattern (Fig. 1c), indicating that there was no reaction and/or inter-diffusion of elements between cathode and electrolyte. These results reveal that $La_2NiO_{4+\delta}$ has good chemical compatibility with the LSGM electrolyte under IT-SOFC operation conditions.

The variation of the open-circuit voltage (OCV) for the $La_2NiO_{4+\delta}$/LSGM/SDC/Ni–SDC single cell in humidified hydrogen (3% H_2O) and air as a function of the temperature is illustrated in Fig. 2. The OCV is 1.12 V at 600 °C and decreases with increasing temperature (1.07 V at 850 °C). These OCVs are close to the theoretical values; indicating a good densification of the LSGM electrolyte and no gas leakage after reduction of the anode.

Fig. 3 shows voltage and power density as a function of current density for the $La_2NiO_{4+\delta}$/LSGM/SDC/Ni–SDC cell, in humidified hydrogen and static air, at different temperatures (from 600 to 850 °C). It is observed that the cell voltage linearly decreases with increasing current density; there is a rapid drop because of electrode polarisation indicates good electrodes performance. The maximum power densities were 23, 51, 91, 160, 226, and 322 mW cm^{-2} at 600, 650, 700, 750, 800 and 850 °C, with the current densities of 46, 102, 169, 288, 429 and 601 mA cm^{-2}, respectively. Considering the thickness of the electrolyte ~400 μm, the cell performance is encouraging; one would expect higher power densities to be achieved using a thin-film electrolyte.

The impedance spectra for the $La_2NiO_{4+\delta}$/LSGM/SDC/Ni–SDC single cell under open circuit voltage in H_2 (3% H_2O) and static air at different temperatures are shown in Fig. 4. At temperatures lower than 800 °C, the Nyquist diagrams present part of the first arc at high-frequency region associated with the grain boundary of the electrolyte and a depressed arc in the low-frequency region. The asymmetrical characteristics of the depressed arc revealed at least two electrode contributions. In contrast, the spectra at 800 and 850 °C show two depressed arc contributions with peak frequencies of 257 and 0.15 Hz. The lower-frequency electrode arc did not make a second intercept with the real axis in the frequency range. The impedance data were fitted to the equivalent circuit of the type $R_o(R_1Q_1)(R_2Q_2)$, where R_o is the ohmic resistance of cell (mainly associated with the LSGM electrolyte), and the remaining components are associated with two interfaces: the cathode–electrolyte interface and the anode–electrolyte interface. The first component (R_1Q_1) appears as a semi-circle at the high/medium frequency region and the second one, (R_2Q_2), at the low frequency region. The fitting was performed with ZView software [33]. It is noted that the data associated with the grain boundary were omitted. Based on the fitted arcs, the polarisation resistance of electrodes (total width of the arcs) was calculated as the sum of R_1 and R_2, and the total resistance of the cell as the sum of the ohmic resistance and the polarisation resistance.

The polarisation resistance values were 7.45, 3.44, 1.53, 0.77, 0.48 and 0.31 Ω cm^2 at 600, 650, 700, 750, 800 and 850 °C, respectively. Furthermore, Fig. 5 displays the total cell resistance (R_t),

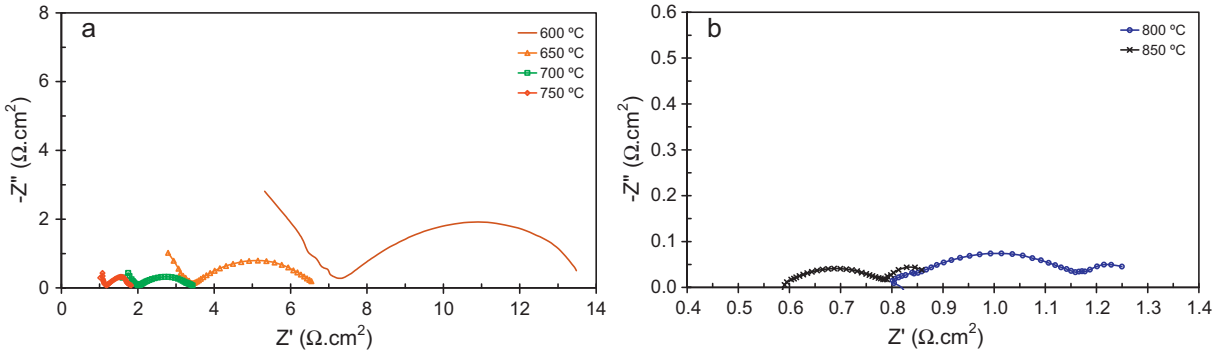

Fig. 4. Impedance spectra for the $La_2NiO_{4+\delta}$/LSGM/SDC/Ni–SDC cell measured in H_2 and static air under open-circuit condition at different temperatures: (a) 600, 650, 700 and 750 °C; (b) 800 and 850 °C.

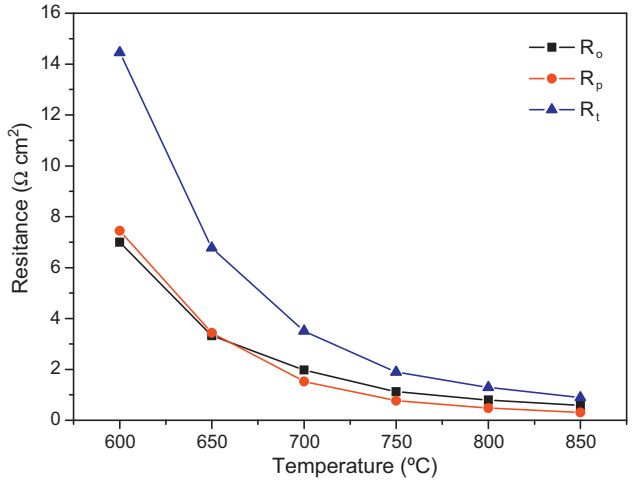

Fig. 5. Total cell resistances (R_t), polarisation resistances (R_p), and ohmic resistances (R_o), obtained from the fitting of impedance data at different temperatures of the $La_2NiO_{4+\delta}$/LSGM/SDC/Ni–SDC cell.

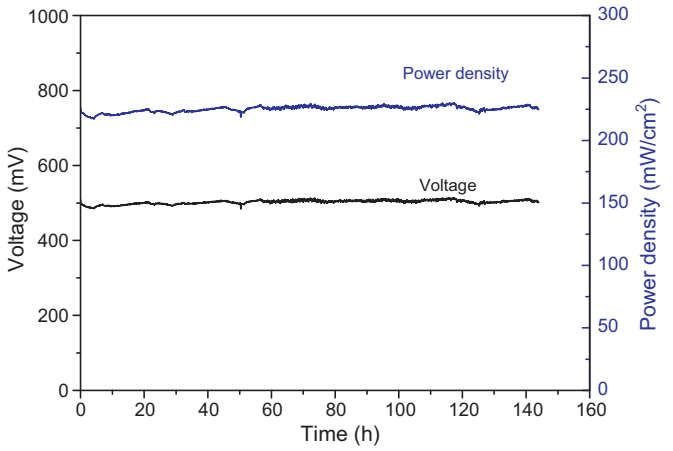

Fig. 6. Voltage and power density versus time, under a constant current of 448 mA cm^{-2}, at 800 °C in H_2 (3% H_2O) as function of time.

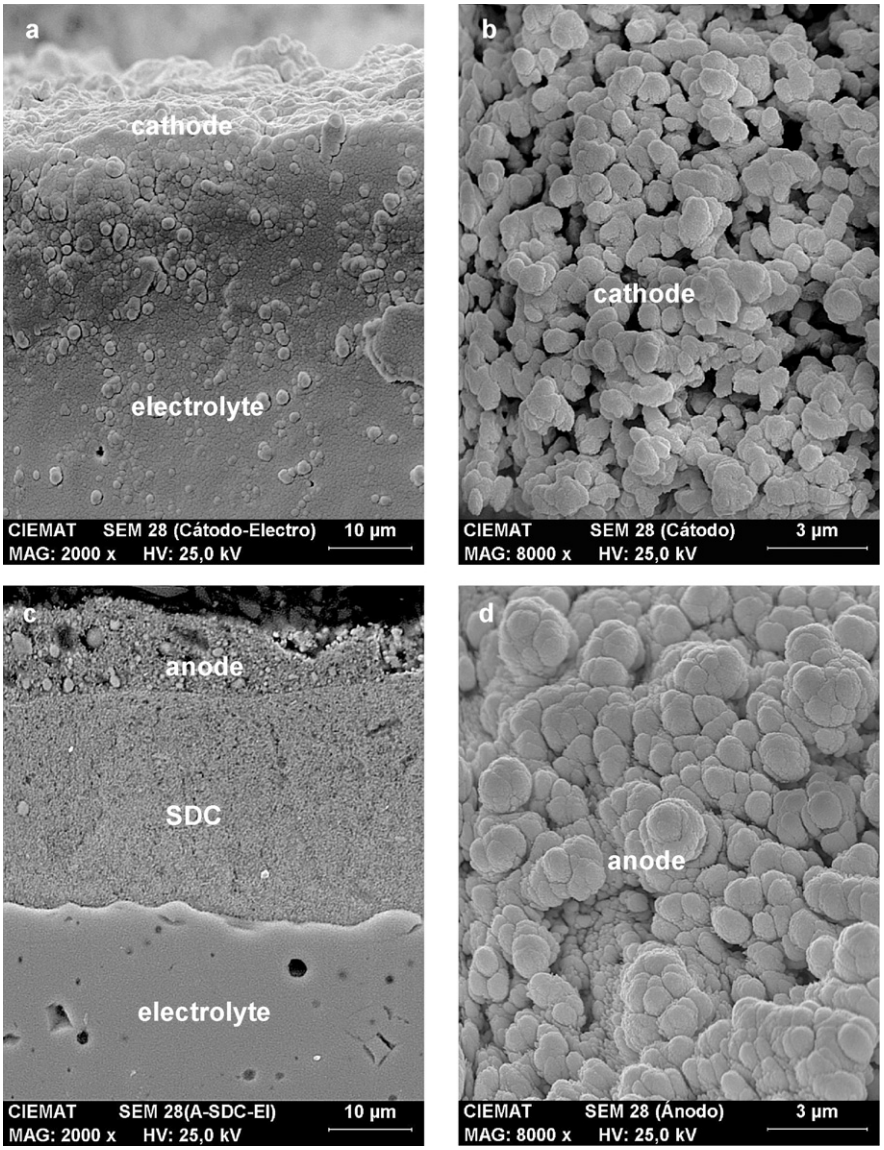

Fig. 7. SEM images of the $La_2NiO_{4+\delta}$/LSGM/SDC/Ni–SDC cell after testing. (a) Cross-sectional of $La_2NiO_{4+\delta}$/LSGM; (b) cathode surface; (c) cross-sectional of Ni–SDC/SDC/LSGM; (d) anode surface.

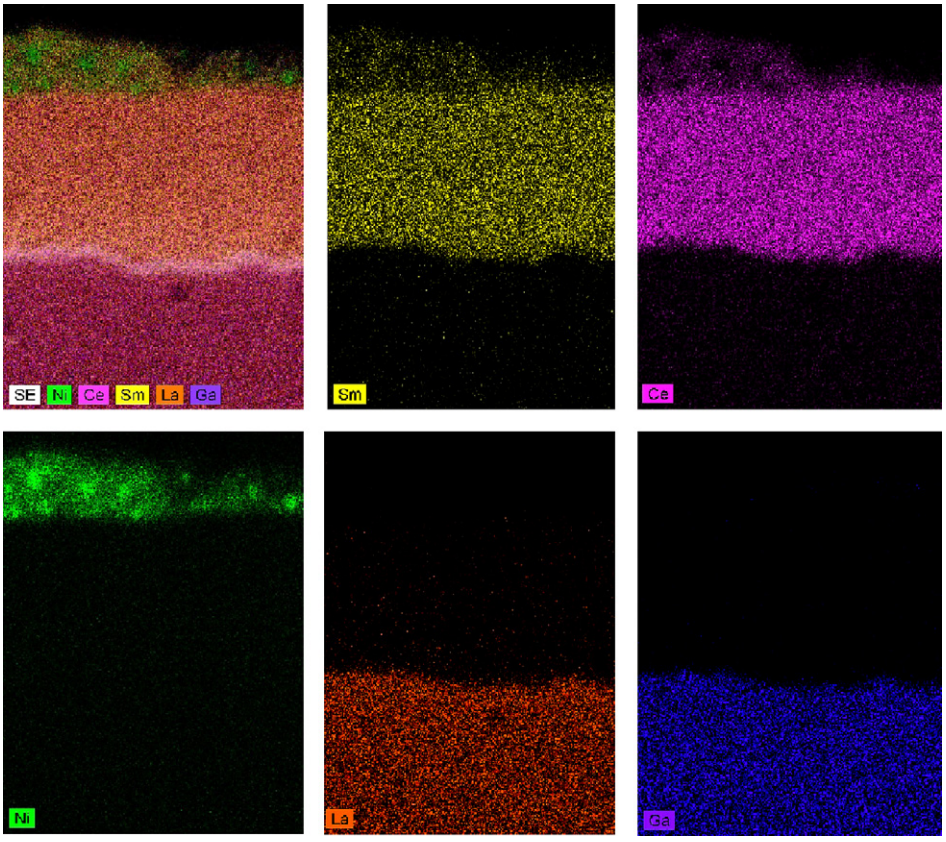

Fig. 8. EDX mapping of the anode–electrolyte interface. Yellow: Sm, magenta: Ce, green: Ni, orange: La, blue: Ga. (For interpretation of the references to color in this figure legend, the reader is referred to the web version of the article.)

electrode polarisation resistance (R_p) and cell ohmic resistance (R_o). It can be seen that all resistances significantly decrease with an increase in operating temperature. When the temperature decreased from 850 to 600 °C, the ohmic resistance increased around 12 times, while the polarisation resistances increase about 24 times. The values of R_p and R_o are roughly comparable at 650 and 600 °C which implies that the effect of polarisation resistance is more important for cell performance at low operating temperature. The ohmic contribution of the total cell resistance, mainly due to the electrolyte resistance, increases from 48% at 600 °C to 65% at 850 °C, and is dominant at higher temperatures. However, it is important to point out that a reduction of the electrolyte thickness will reduce the ohmic resistance and could enhance considerably the cell performance. In addition, the electrode processing could be optimised through depositing using techniques like screen printing, that could reduce the polarisation resistance, and enhanced further the efficiency of the cell.

The stability of the single cell was tested at 800 °C for 144 h, under a constant density current of 448 mA cm^{-2}, as shown in Fig. 6. The cell voltage dropped around 498 mV and generates a power density of ~220 mW cm^{-2}, remaining stable across the period. These values are in good agreement with those shown in Fig. 2. In order to confirm the system stability, a comparison of polarisation curves and impedance spectra before and after durability test was carried (data not shown). The values of voltage, power density and total resistance of cell had hardly changed; these results give evidence of the absence of significant cell degradation.

Fig. 7 illustrates the cross-sectional SEM micrographs of the $La_2NiO_{4+\delta}$/LSGM and Ni–SDC/SDC/LSGM interfaces, as well as the cathode and anode surfaces after single cell evaluation. They were obtained by fracturing the cell, setting it in resin and polishing the exposed cross-sectional surface. The LSGM electrolyte film was essentially dense, with a continuous and crack-free surface morphology and no open pinholes. In general, both electrodes exhibit a homogeneous porous microstructure, showing uniform and clear grains with an average grain size of ~0.7 and 1.1 μm for cathode and anode, respectively. The cathode layer is well-adhered to the LSGM electrolyte and presents high interfacial connectivity (Fig. 7a). To minimise the reaction between the Ni–SDC anode and the LSGM electrolyte a SDC buffer layer was painted onto the anode side of the electrolyte. It can be identified in Fig. 7c as the interlayer between LSGM electrolyte and Ni–SDC anode in SOFC unit cell. The EDX mapping of Ni, Ga and La elements revealed neither the presence of Ni on the electrolyte nor Ga and La elements on the anode area (Fig. 8). Therefore, it can be concluded that SDC layer successfully acts as a barrier hindering the contact between nickel and electrolyte material. The thickness and morphology of this intermediate layer was enough to avoid the chemical reaction to form the insulating $LaNiO_3$ and $LaSrGa_3O_7$ phases and thus reducing the anode polarisation resistance, improving the durability and performance of the single cell.

4. Conclusions

The $La_2NiO_{4+\delta}$ compound has been investigated as cathode material for potential application to IT-SOFC with the LSGM electrolyte. XRD results show that no reaction product is found between $La_2NiO_{4+\delta}$ and LSGM after heat-treatment at 1000 °C for 50 h. A single cell of four layers, $La_2NiO_{4+\delta}$ cathode, dense LSGM electrolyte, SDC barrier layer, and Ni–SDC anode was fabricated and tested in humidified H_2 (3% H_2O) as fuel, and stationary air as oxidant in the temperature range 600–850 °C. The maximum power densities of the cell with about 400 μm thick electrolyte, were 160, 226, and 322 mW cm^{-2} at 750, 800 and 850 °C, with the

polarisation resistances of 0.77, 0.48 and 0.31 $\Omega\,cm^2$ at the corresponding temperatures. The performance of the single cell was increased at higher temperatures due to the decrease in the total cell resistance. Impedance data analysis revealed that the electrodes polarisation resistance (R_p) and the ohmic resistance (R_o) contribute practically equally to the total cell resistance at 600 and 650 °C. The influence of R_p in the total cell resistance decreases at increasing the temperature. Cell stability tests indicated no degradation of performance after testing during 144 h at 800 °C under a load demand of 448 mA cm^{-2}. The cell performance may be further improved by reducing the electrode thickness and optimizing the electrode processing. These results indicate that $La_2NiO_{4+\delta}$ cathode with LSGM electrolyte is a suitable material system for IT-SOFC.

Acknowledgement

This work was supported by the Community of Madrid (Project DIVERCEL; Ref. S2009/ENE-1475).

References

[1] H.Y. Jung, K.S. Hong, H. Kim, H.R. Lim, J.-W. Son, J. Kim, H.W. Lee, J.H. Lee, J. Electrochem. Soc. 154 (5) (2007) B480–B485.
[2] K. Kawahara, S. Suda, M. Suzuki, M. Kawano, H. Yoshida, T. Inagaki, Solid State Ionics 180 (2009) 236–240.
[3] T. Ishihara, H. Matsuda, Y. Takita, J. Am. Chem. Soc. 116 (1994) 3801.
[4] M. Feng, J.B. Goodenough, Eur. J. Solid State Inorg. Chem. 31 (1994) 663–672.
[5] W. Gong, S. Gopalan, U.B. Pal, J. Electrochem. Soc. 152 (9) (2005) A1890–A2189.
[6] K. Huang, J.-H. Wan, J.B. Goodenough, J. Electrochem. Soc. 148 (7) (2001) A788–A794.
[7] J.M. Haag, B.D. Madsen, S.A. Barnett, K.R. Poeppelmeier, Electrochem. Solid-State Lett. 11 (4) (2008) B51–B53.
[8] J.H. Kim, A. Manthiram, J. Electrochem. Soc. 155 (4) (2008) A385–B390.
[9] J. Yan, H. Matsumoto, M. Enoki, T. Ishihara, Electrochem. Solid-State Lett. 8 (8) (2005) A389–A391.
[10] J. Feig, J. Maer, J. Eur. Ceram. Soc. 24 (2004) 1343–1347.
[11] S.C. Singhal, K. Kendall, High Temperature Solid Oxide Fuel Cells: Fundamentals, Design and Applications, Elsevier, Oxford UK, 2003, p. 257.
[12] P. Hjalmarsson, M. Søgaard, A. Hagen, M. Mogensen, Solid State Ionics 179 (2008) 636–646.
[13] F. Tietz, V.A.C. Haanappel, A. Mai, J. Mertens, D. Stöver, J. Power Sources 156 (2006) 20–22.
[14] C. Xia, W. Rauch, F. Chen, M. Liu, Solid State Ionics 149 (2002) 11–19.
[15] J. Peña-Martínez, D. Marrero-López, D. Pérez-Coll, J.C. Ruiz-Morales, P. Nuñez, Electrochim. Acta 52 (2007) 2950–2958.
[16] K.K. Hansen, K. Vels Hansen, Solid State Ionics 178 (2007) 1379–1384.
[17] K.T. Lee, A. Manthiram, J. Electrochem. Soc. 153 (4) (2006) A794–A798.
[18] J.M. Ralph, C. Rossignol, R. Kumar, J. Electrochem. Soc. 150 (2003) A1518–A1522.
[19] H. Zhao, F. Mauvy, C. Lalanne, J.-M. Bassat, S. Fourcade, J.-C. Grenier, Solid State Ionics 179 (2008) 2000–2005.
[20] S.J. Skinner, J.A. Kilner, Solid State Ionics 135 (2000) 709–712.
[21] M. Al Daroukha, V.V. Vashooka, H. Ullmanna, F. Tietzb, I. Arual Raj, Solid State Ionics 158 (2003) 141–150.
[22] S.-W. Baek, J.H. Kim, J. Bae, Solid State Ionics 179 (2008) 1570–1574.
[23] F. Mauvy, C. Lalanne, J.M. Bassat, J.C. Grenier, H. Zhao, P. Dordor, Ph. Stevens, J. Eur. Ceram. Soc. 25 (2005) 2669–2672.
[24] A. Aguadero, M.J. Escudero, M. Pérez, J.A. Alonso, V. Pomjakushinc, L. Daza, Dalton Trans. (2006) 4377–4383.
[25] J. Wan, J.B. Goodenough, J.H. Zhu, Solid State Ionics 178 (2007) 281–286.
[26] V.V. Kharton, E.V. Tsipis, A.A. Yaremchenkoa, J.R. Frade, Solid State Ionics 166 (2004) 327–337.
[27] A.L. Shaula, E.N. Naumovich, A.P. Viskup, V.V. Pankov, A.V. Kovalevsky, V.V. Kharton, Solid State Ionics 180 (2009) 812–816.
[28] A. Aguadero, M. Pérez, J.A. Alonso, L. Daza, J. Power Sources 151 (2005) 52–56.
[29] A. Aguadero, J.A. Alonso, M.J. Escudero, L. Daza, Solid State Ionics 179 (2008) 393–400.
[30] A. Aguadero, J.A. Alonso, M.T. Fernández-Díaz, M.J. Escudero, L. Daza, J. Power Sources 169 (2007) 17–24.
[31] A. Aguadero, J.A. Alonso, M.J. Martínez-Lope, M.T. Fernández-Díaz, M.J. Escudero, L. Daza, J. Mater. Chem. 16 (2006) 3402–3408.
[32] P. Huang, A. Petric, J. Electrochem. Soc. 143 (1996) 1644–1648.
[33] ZPlot for Windows Version 2.1, Scribber Associates Inc., 1999.